On the estimation of spatial averaging volume for determining stress using atomistic methods

Manfred H. Ulz[1], Kranthi K. Mandadapu[2] and Panayiotis Papadopoulos[3,*]

[1]Institute for Strength of Materials, Graz University of Technology, Kopernikusgasse 24/I, 8010 Graz, Austria

[2]Sandia National Laboratories, Livermore, California 94551-0969, USA

[3]Department of Mechanical Engineering, University of California, Berkeley, California 94720-1740, USA

E-mail: `panos@berkeley.edu`

Abstract. The estimation of stress at a continuum point from the atomistic scale requires volume averaging over a region that contains this point. A hypothesis is put forth to obtain a lower bound for the size of this region based on an analogy to the Ising model. This hypothesis is tested on copper using two classical elasticity problems.

Submitted to: *Modelling Simulation Mater. Sci. Eng.*

1. Introduction

In continuum mechanics, stress is a local quantity defined using a limiting process known as Cauchy's tetrahedron argument [1]. To reconcile the local stress of continuum mechanics with the interaction forces of atomistic mechanics, one typically resorts to volume averaging at the atomistic scale. In this case, the length scale involved in the averaging process becomes crucial. Therefore, it is desirable to develop rational guidelines for the estimation of such a length scale.

Atomistic definitions of stress date back to Cauchy, who considered a plane through a point and investigated the forces of interacting particles crossing the plane inside a certain radius from this point, see [2, Note B]. Another milestone is the pioneering work by Irving and Kirkwood [3], who derived pointwise definitions of stress and heat flux based on phase space averaging of extensive quantities, namely mass, momentum and energy. Irving and Kirkwood's procedure was subsequently modified in [4, 5] by introducing spatial localization functions that effect weighted volumetric averaging.

When the interaction forces are averaged over an extremely small volume, the resulting atomistic stress exhibits wide spatial variations which are inconsistent with

* Author to whom any correspondence should be addressed.

the smooth continuum stress. On the other hand, when the averaging volume is too large, the resulting atomistic stress is excessively smeared and fails to capture potential inhomogeneities in the continuum stress. Between the preceding two extremes, one may conjecture that there exists a range of averaging volumes to which the atomistic stress is essentially insensitive. The existence of such an intermediate asymptotic range is argued by Barenblatt in a more general context in [6, Chapter 2].

In current practice, the averaging volume is generally chosen by calibrating it against existing analytical solutions for stress. The aim of this paper is to propose a lower bound for the characteristic length of the spatial averaging volume used in the calculation of atomistic stress. For any such bound to be rationally defined, it must be expressed as a function of some inherent length scale of the problem. Here, the proposed hypothesis is motivated by the Ising model of statistical mechanics and states that the lower bound of the characteristic length is a multiple of the correlation length of the potential energy in the atomistic system.

The organization of the paper is as follows: Section 2 includes a brief review of the Irving-Kirkwood and Hardy definitions of stress. This is followed in Section 3 by the statement of the proposed hypothesis for the lower bound of the averaging volume. This hypothesis is next applied to copper in Section 4, and its validity is tested in Section 5 by way of two elasticity problems.

2. Atomistic stress

In their seminal paper [3], Irving and Kirkwood laid the foundation for the definition of continuum stress and heat flux fields in terms of microscopic kinematics and kinetics. Many commonly used atomistic definitions of stress may be considered as amendments or variations of their formula. Although Irving and Kirkwood define stress pointwise by Dirac delta functions, they state in their paper that macroscopic stress must be obtained by spatial averaging. In particular, this averaging needs to be performed over a microscopically large, but macroscopically small, domain determined by the inherent length scale of the microstructure and the resolution of one's measuring instruments. In a subsequent work [7], Noll slightly reformulated Irving and Kirkwood's stress formula by replacing an infinite series term with a closed-form integral expression.

The Irving and Kirkwood stress formula gives rise to the virial stress $\boldsymbol{\sigma}_v$ at a continuum point $\mathbf{x}$ upon neglecting all higher-order terms in the expansion of Dirac-delta differences and averaging over a volume $\Omega(\mathbf{x})$ centered at point $\mathbf{x}$. This is expressed as

$$\begin{aligned}\boldsymbol{\sigma}_v(\mathbf{x}) \;=\; & -\frac{1}{\Omega(\mathbf{x})}\Bigg(\sum_{i=1}^{N} m_i \mathbf{u}_i \otimes \mathbf{u}_i + \frac{1}{2!}\sum_{i,j=1,j\neq i}^{N} \mathbf{f}_{ij} \otimes \mathbf{x}_{ij} \\ & + \frac{1}{3!}\sum_{i,j,k=1,k\neq j\neq i}^{N} \mathbf{f}_{ijk} \otimes (\mathbf{x}_{ij} + \mathbf{x}_{ik}) + \dots\Bigg)\,. \end{aligned} \tag{1}$$

Here, N is the number of atoms in $\Omega(\mathbf{x})$, m_i the mass of atom i, $\mathbf{u}_i$ the velocity of atom i relative to the mean velocity of the N atoms, and $\mathbf{x}_{ij} = \mathbf{x}_i - \mathbf{x}_j$ with $\mathbf{x}_i$ being the

position vector of atom i. Also, $\mathbf{f}_{ij}$ and $\mathbf{f}_{ijk}$ denote forces on atom i due to its pair and three-body interactions with other atoms. The stress in Equation (1) becomes equal to the one derived from the virial theorem of [8–10] by replacing $\Omega(\mathbf{x})$ with the total volume V of the system.

The Hardy stress [4, 5] is derived from [3] by replacing the Dirac delta function for atom i in the stress definition with a localization function $\psi(\mathbf{x}-\mathbf{x}_i)$ which leads to

$$\begin{aligned}\boldsymbol{\sigma}_h(\mathbf{x}) \;=\; -\Bigg(&\sum_{i=1}^{N} m_i\mathbf{u}_i\otimes\mathbf{u}_i\psi(\mathbf{x}-\mathbf{x}_i)+\frac{1}{2!}\sum_{i,j=1,j\neq i}^{N}\mathbf{f}_{ij}\otimes\mathbf{x}_{ij}B_{ij}(\mathbf{x})\\&+\frac{1}{3!}\sum_{i,j,k=1,k\neq j\neq i}^{N}\mathbf{f}_{ijk}\otimes\Big(\mathbf{x}_{ij}B_{ij}(\mathbf{x})+\mathbf{x}_{ik}B_{ik}(\mathbf{x})\Big)+\ldots\Bigg)\,. \qquad (2)\end{aligned}$$

The function $\psi(\mathbf{x}-\mathbf{x}_i)$ is non-negative, reaches a maximum at $\mathbf{x}=\mathbf{x}_i$, and tends to zero as the distance $|\mathbf{x}-\mathbf{x}_i|$ becomes large. Furthermore, it has to be normalized such that $\int_{\mathcal{R}}\psi(\mathbf{x}-\mathbf{x}_i)\,\mathrm{d}\Omega=1$, where $\mathcal{R}$ is the region occupied by the system. This function smears out the discrete nature of matter and also defines the region around a continuum point $\mathbf{x}$ over which space averaging is performed. The bond function $B_{ij}(\mathbf{x})$ between atoms i and j is defined in Equation (2) as $B_{ij}(\mathbf{x})=\int_0^1\psi(\mathbf{x}-\mathbf{x}_i+\lambda\mathbf{x}_{ij})\,\mathrm{d}\lambda$. This function defines the contribution to stress due to the interaction of atoms i and j according to the portion (and corresponding weight) of the line segment (defined by i and j) that crosses the space-averaging volume. A comprehensive overview of atomistic stress measures is given in [11, 12].

3. A hypothesis for the spatial averaging volume

Equations (1) and (2) show that the continuum stress at a point $\mathbf{x}$ is calculated either by averaging over a volume around $\mathbf{x}$ or by integrating over the support of a localization function centered at $\mathbf{x}$. As noted in the Introduction, the averaging volume (likewise, the support of the localization function) should be sufficiently large to eliminate the noise in stress due to the individual atomistic interactions and sufficiently small to preserve the physically relevant spatial variations in stress. Therefore, it is essential to define a suitable volume or localization function for such a calculation. In this section, a hypothesis is proposed that informs the choice of these two entities. This hypothesis is based on the spatial correlations of the potential energy and is inspired by the classical Ising model of statistical mechanics [13, Chapter 3].

By way of background, recall that the Ising model is defined on a set of N variables s_i, called the spins, each of which has value $+1$ or -1. The Hamiltonian for this system may be written as

$$\tilde{\mathcal{H}} \;=\; -\sum_{i=1}^{N}H_is_i-\frac{1}{2!}\sum_{i,j=1,j\neq i}^{N}J_{ij}s_is_j-\frac{1}{3!}\sum_{i,j,k=1,k\neq j\neq i}^{N}K_{ijk}s_is_js_k-\ldots\,. \qquad (3)$$

Here, the magnetic field H_i, the pair coupling J_{ij} and the three-spin coupling K_{ijk} describe the interactions of spin i with the external field, with spin j and with the spins

(j,k), respectively. When the Hamiltonian is restricted to nearest-neighbor interactions, the two-point correlation $\Big\langle (s_i - \langle s_i \rangle)(s_j - \langle s_j \rangle) \Big\rangle$, which defines the correlation in the fluctuation of the spins s_i and s_j, may be computed analytically and is shown to decay exponentially to zero as a function of the "distance" $\mid i - j \mid$ [13, Section 3.5]. This means that fluctuations in s_i affect the values of s_j only inside a small neighborhood of i. Note that the angled brackets in the preceding definition of the two-point correlation denote phase-space averaging.

Next, turning to an atomistic N-particle system, a Hamiltonian may be written as

$$\mathcal{H} = \frac{1}{2}\sum_{i=1}^{N} \frac{1}{m_i}\mathbf{p}_i \cdot \mathbf{p}_i + \sum_{i=1}^{N} U_i + \frac{1}{2!}\sum_{i,j=1,j\neq i}^{N} U_{ij} + \frac{1}{3!}\sum_{i,j,k=1,k\neq j\neq i}^{N} U_{ijk} + \dots \,, \quad (4)$$

as, e.g., in [14]. Here, m_i and $\mathbf{p}_i$ are the mass and momentum of atom i, respectively. Also, U_i denotes the potential due to an external field acting on atom i, while U_{ij} and U_{ijk} denote the pair and cluster potentials due to the interaction of atom i with j and with the pair (j,k), respectively. The preceding Hamiltonian may be also written as $\mathcal{H} = \sum_{i=1}^{N} E_i$, where E_i is the total energy of particle i. This, in turn, may be expressed as $E_i = T_i + V_i$, where T_i and V_i are the kinetic and potential energies of particle i, defined respectively as

$$T_i = \frac{1}{2m_i}\mathbf{p}_i \cdot \mathbf{p}_i \quad (5)$$

and

$$V_i = U_i + \frac{1}{2!}\sum_{j\neq i}^{N} U_{ij} + \frac{1}{3!}\sum_{j,k\neq i}^{N} U_{ijk} + \dots \,. \quad (6)$$

It is clear that Equations (3) and (4) share the same general additive structure for the interaction terms. Furthermore, it is assumed here that fluctuations in the total energy of a particle satisfy the same correlation property as the spins in the Ising model. This may be viewed as a statement of locality, as remarked in [15, Section III]. Drawing from the analogy between the Ising and the N-particle Hamiltonians, a hypothesis is put forth according to which a lower bound for the length (hence, also for the volume) used in spatial averaging at a point $\mathbf{x}_i$ occupied by atom i is determined by the decay of the two-point correlation of the energy $\Big\langle (E_i - \langle E_i \rangle)(E_j - \langle E_j \rangle) \Big\rangle$, for atoms $j \neq i$. This will be referred to as the correlation length at atom i. For the more general case of a point $\mathbf{x}$ not occupied by an atom, the correlation length is equal to that obtained for the nearest atom i.

The preceding hypothesis may be further refined upon noting that for a system in thermodynamic equilibrium at a fixed temperature, the particle velocities follow the canonical distribution [16]. This readily implies that the two-point correlation of the kinetic energy vanishes. Therefore, only the two-point correlation $\Big\langle (V_i - \langle V_i \rangle)(V_j - \langle V_j \rangle) \Big\rangle$ of the potential energy is of relevance in the determination of the averaging volume.

The proposed hypothesis enables the estimation of the spatial averaging volume at each continuum point of interest according to the local microstructure. However,

this estimation demands a considerable amount of computation time. Therefore, it is advisable to determine a correlation length of the material under idealized conditions, which can be subsequently used to define the spatial averaging volume.

4. Correlation length in copper under idealized conditions

This section describes the procedure by which the spatial correlation of potential energy is used to determine a correlation length for copper.

A face-centered cubic lattice with periodic boundary conditions and $8 \times 8 \times 8$ unit cells is modeled using LAMMPS [17]. The unit cell length is taken to be $a = 3.615$ Å and an EAM potential, given by

$$\mathcal{H} \;=\; \frac{1}{2}\sum_{i=1}^{N}\frac{1}{m_i}\mathbf{p}_i\cdot\mathbf{p}_i + \sum_{i=1}^{N}F\Bigg(\sum_{j=1,j\neq i}^{N}\rho(x_{ij})\Bigg) + \frac{1}{2!}\sum_{i,j=1,j\neq i}^{N}U_{ij}\;, \tag{7}$$

is used to determine the atomic interactions with cut-off radius of $2.5a$ [18, 19]. Here, $\rho(x_{ij})$ is the contribution to the electron density from atom j at atom i with x_{ij} being the distance between the two atoms, and $F(\cdot)$ is an embedding function that denotes the energy required to place atom i into the existing electron cloud. Standard forms of these functions may be found in [19, Appendix A]. It follows that the energy of atom i is given by

$$E_i \;=\; \frac{1}{2m_i}\mathbf{p}_i\cdot\mathbf{p}_i + F\Bigg(\sum_{j=1,j\neq i}^{N}\rho(x_{ij})\Bigg) + \frac{1}{2!}\sum_{j=1,j\neq i}^{N}U_{ij} \tag{8}$$

while the Hardy stress is derived using the Irving-Kirkwood procedure [3–5] to be

$$\begin{aligned}\boldsymbol{\sigma}_h(\mathbf{x}) \;=\; & -\sum_{i=1}^{N} m_i\mathbf{u}_i\otimes\mathbf{u}_i\psi(\mathbf{x}-\mathbf{x}_i) + \\ & \sum_{i,j=1,j\neq i}^{N}\Bigg[F'\Bigg(\sum_{l=1,l\neq i}^{N}\rho(x_{il})\Bigg)\frac{\rho'(x_{ij})}{x_{ij}}\mathbf{x}_{ij} - \mathbf{f}_{ij}\Bigg]\otimes\mathbf{x}_{ij}B_{ij}(\mathbf{x})\;,\end{aligned} \tag{9}$$

where the superscript $'$ denotes the derivative of a function with respect to its argument. The corresponding virial stress is obtained from (9) by replacing the localization function ψ and the bond function B_{ij} by Ω, as in Equation (1).

The calculation of correlation length consists of three steps: First, the system is equilibrated at a temperature of 300 K using the Nosé-Hoover algorithm [20] for 400,000 time steps with step-size of 1 fs. Next, the atoms are tracked for 48 million additional time steps with the same step-size, where the state at every third time step is used for the calculation of correlation functions. Finally, an arbitrary atom i in the bulk system is chosen to compute the spatial correlation function C_{ij} as

$$C_{ij}(s) \;=\; \langle\delta E_i(0)\delta E_j(s)\rangle \;=\; \frac{1}{M}\sum_{m=0}^{M-1}\delta E_i(m\Delta t)\delta E_j(m\Delta t+s)\;, \tag{10}$$

where $\delta E_i(s)$ is the fluctuation in the atom's energy from its average at time $t = s$ [21, Chapters 11 and 35]. Here, this atom is chosen to be at the center of the system and spatial correlations of potential energy are computed with its neighbors. Also, the variable s in Equation (10) is set to zero since attention is focused on steady-state problems.

The correlation of the potential energy between the atom at the center of the system and its neighbors is shown in Figure 1. The plot reveals non-zero correlation up to a distance of approximately $2.00a$. Therefore, the hypothesis in Section 3 implies that the length scale of the averaging volume (which is taken here to be twice the correlation length) is of the order of $4a \doteq 14.5$ Å, a remarkably small size. Note that the observed correlation length is smaller than the cut-off radius employed in the empirical potential. In fact, it is found by numerical experimentation that the correlation length remains unchanged even when the cut-off radius is increased to $3a$ or $4a$. Also, Figure 1 confirms that the kinetic energy of any two distinct atoms is uncorrelated.

The magnitude of the potential energy correlation function depends on temperature, as seen in Figure 2. Specifically, with the exception of the closest neighbors, the correlation decreases with increasing temperature. However, the correlation length remains the same over a range of temperatures.

There is a small influence on the correlation by the type and magnitude of loading within the realm of small deformations. This influence is observed by estimating the correlations in a deformed lattice at 300 K. First, the system is compressed without lateral expansion by reducing the unit cell length to simulate axial strains of 1% and 5%. Next, the influence of simple shear is investigated by deforming the unit cell accordingly to generate shears of 1% and 5%. The results for both loading cases are given in Figure 3. The dependence of the correlations on deformation may be explained by the changes in the lattice topology. Again, the correlation length itself does not appear to be significantly affected by the deformation.

The correlation results do not appear to be affected by the size of the system. Indeed, it can be seen from Figure 4 that the results of the base calculation on $48\times48\times48$ unit cells do not differ in any substantial way from those of the original $8 \times 8 \times 8$ case at the end of 6 million time steps. This is expected, to some extent, due to the use of periodic boundary conditions to simulate the bulk system.

Surface effects on the correlations are investigated by considering an fcc lattice of copper with size of $8 \times 8 \times n$ unit cells, where $n = 24, 48$. Traction-free (non-periodic) boundary conditions are applied on the surface with 8×8 unit cells, while periodic boundary conditions are imposed on the other surfaces. Correlations are computed for the center atom on the free-boundary face and are compared to the base periodic case. The results at the end of 6 million time steps show an influence of surface effects on correlations, as seen in Figure 4. This can be explained by observing that the atoms close to the surface are subject to end-effects, which generate stresses in a small region around the surface. However, the correlation lengths remain essentially the same even in the presence of free surfaces. This is because the strains in the vicinity of the surface

are relatively small, and, as already seen in Figure 3, the correlation lengths for small strains remain practically unchanged.

Similar results are found for the case of aluminum modeled again using the EAM potential. However, these are not included here due to space limitations.

5. Examples

This section includes numerical simulations that test the validity of the proposed averaging hypothesis. The simulations focus on the virial and Hardy stress obtained from atomistic data using different sizes of the spatial averaging volume. The two representative problems analyzed here are a crystal with an edge dislocation and an infinite plate with a circular notch under uniaxial load (Kirsch problem). Both problems possess analytical solutions in elasticity theory. As stress is a continuum concept, the atomistic definitions should reproduce those solutions satisfactorily, albeit not exactly due to the use of finitely sized atomistic domain.

All simulations are performed at zero temperature, which cancels the influence of the kinetic part of the stress. The conjugate gradient method is used to minimize the total potential energy of the system.

5.1. Edge dislocation

The distribution of residual stress about the core of an edge dislocation in an elastic solid is considered here as an introductory example. The stress is exclusively due to the defect in the absence of external loading or inhomogeneities. The material is taken to be a single crystal of copper in an fcc lattice. The arrangement of atoms in the vicinity of the dislocation relative to the coordinate system is illustrated in Figure 5. An analytical solution of this problem within the theory of anisotropic linear elasticity is included in [22]. Here, the elastic constants are taken from experimental measurements at room temperature [23], and are $c_{11} = 171.00$ GPa, $c_{12} = 123.90$ GPa and $c_{44} = 75.60$ GPa following the convention in [24]. A molecular dynamics simulation of this problem is found in [25].

In this example, the atomistic model of the solid consists of $1000 \times 1000 \times 3$ unit cells with periodic boundaries on the two square surfaces and free boundaries on the remaining four surfaces. The edges of the solid are aligned to the crystallographic axes (with the x_1-axis coinciding with [100]) and a $\langle 100 \rangle$ edge dislocation is created at the center of the simulation box by removing one column of corner atoms and an adjacent column of face atoms, and subsequently closing the gap by relocating atoms near the dislocation in order to bring the system closer to the ultimate equilibrium state. This produces a Burgers vector oriented along the x_1-direction. Subsequently, energy minimization at zero temperature with relative tolerance 10^{-15} leads the system to equilibrium.

The distribution of virial normal stresses σ_{11} and σ_{22} along the x_2-axis, as well as

the virial shear stress σ_{12} along the x_1-axis starting from the dislocation core are shown in Figure 6. Corresponding results for the Hardy stress are shown in Figure 7. The analytical solution is also plotted for reference purposes. Both the virial and Hardy stresses are evaluated at points with coordinates 0, $3/5a$, $6/5a$, etc. on either the x_1- or x_2-axis. Owing to the periodic boundary conditions, the averaging volume Ω at each such point is an infinite cylinder whose major axis is perpendicular to the (x_1, x_2)-plane. Here, cylinders of radii $0.75a$, $1.25a$, $1.75a$, $2.00a$, $2.25a$, $2.75a$ and $5.00a$ are considered for the evaluation of stresses. A constant localization function is chosen for the Hardy stress to be as close as possible to the virial stress. Additional calculations, which are not reported here due to space limitations, confirm that the chosen system is large enough for changes to the stresses in the vicinity of the defect with further increases in system size to be practically insignificant.

The virial stress distributions are smooth for all averaging lengths greater than $0.75a$ and exhibit relatively small scattering away from the singularity. However, convergence to the analytical solution is not monotonic with the averaging length. For instance, smaller averaging lengths yield more accurate σ_{11} stress, but less accurate σ_{22} stress relative to the analytical solution. However, the stress distributions for the proposed lower bound averaging length of $2.00a$ derived in Section 4 are reliably accurate for all stress components. The Hardy stress distributions are highly oscillatory for small averaging lengths with large deviations from the analytical solution even further away from the dislocation. However, the magnitude of these oscillations substantially diminishes starting near the averaging length of $2.00a$. As expected, for even larger averaging lengths, the stresses become smoother but deviate significantly from the analytical solution near the singularity.

The comparison of the virial and Hardy stresses to a local analytical solution that involves singularities at the dislocation core is bound to be relevant only starting at some distance away from such singularities. An alternative option of comparing the atomistic stresses to the non-local solution in [26] is not explored here, because the latter incorporates the non-local effect by way of a Gaussian localization function that depends on ad-hoc user-defined parameters.

5.2. Infinite plate with circular notch

In this section, the stress distribution is determined for a plate with a circular notch subject to uniaxial loading. An analytical solution to this problem for the case of plane strain is given in [27] assuming that the plate is infinite and the material is linearly elastic and orthotropic. As in the previous example, this problem is solved for copper, whose elastic parameters are taken again from [23]. An earlier atomistic solution has been given in [11].

A finite section of the plate is modeled by $1000 \times 1000 \times 3$ unit cells with a hole of radius $60a$ placed at the center $(x_1, x_2) = (0, 0)$ of the simulation block. Periodic boundary conditions are imposed on the surfaces normal to the plate. The system is

loaded by applying a uniform tensile traction of $p = 1000$ MPa on the edges normal to the x_2-direction. Homogeneous traction boundary conditions are assumed for the remaining two edges of the plate. Furthermore, the simulation box is oriented along the crystallographic axes with the x_1-axis coinciding with [100]. The equilibrium state is determined at zero temperature by energy minimization with relative tolerance 10^{-15}.

The distribution of axial stresses along the x_1- and x_2-axis is plotted in Figure 8 and Figure 9, respectively, for the virial case and in Figure 10 and Figure 11, respectively, for the Hardy case. All stresses are shown for different cylindrical averaging volumes with constant localization functions (for the Hardy case), and are compared to the analytical solution. Both the virial and Hardy stresses are evaluated at points with coordinates 0, $3/5a$, $6/5a$, etc. on either the x_1- or x_2-axis.

As is evident from the results, this problem entails significant challenges in converging to the analytical stress response. Notwithstanding the obvious difficulty in obtaining smooth stresses close to the notch boundary, significant oscillations are present, especially for the Hardy case, even at considerable distances (of the order of the notch radius itself) from the boundary. As expected, the amplitude of these oscillations is larger for smaller averaging volumes. However, the proposed lower bound averaging length of $2.00a$ already yields reasonable solutions for all reported stresses with a consistent trend of improvement as the averaging length increases. For averaging lengths below this lower bound, the large amplitude of the oscillations prevents the reliable estimation of stress. These observations hold true for both virial and Hardy stresses, although the latter exhibit overall larger amplitudes of oscillation.

It is noted that the small persistent deviation of the numerical results from the analytical solution may be due to the representation of an infinite plate by a relatively small finite system. Still, the size of the system in comparison to the hole radius is chosen to render this deviation practically insignificant.

6. Conclusion

This paper investigates the spatial averaging necessary to deduce continuum stresses from atomistic simulations. In particular, a lower bound for the size of the spatial averaging volume is proposed based on an analogy to the Ising model. This is determined from the decay of the two-point correlation of the potential energy of the atoms. Therefore, the spatial averaging volume surrounding an atom contains all the neighboring atoms that have a non-trivial energetic interaction with it. Numerical experiments in copper indicate that a lower bound to spatial averaging size is at approximately two times the unit cell length, which is a surprisingly small number. Yet, numerical tests on an edge dislocation and a circular notch in an infinite plate support the preceding hypothesis, as they produce virial and Hardy stresses that compare well to the corresponding analytical solutions of elasticity theory.

As a side note, it is observed that the virial and Hardy stress formulations give comparable solutions when space-averaged with length equal or modestly larger than the

proposed lower bound. Although Hardy stress is commonly preferred in the literature and considered to be superior to virial stress, such a conclusion cannot be drawn here on the basis of the findings from the numerical experiments.

Future work needs to focus on simulations at finite temperature and on the effect of the shape of the localization function (especially for space averaging volumes which are close to the proposed lower bound). Finally, it is important to further test the proposed hypothesis on increasingly complex problems, such as those encountered in fracture mechanics.

References

[1] M.E. Gurtin 1981 *An Introduction to Continuum Mechanics* Academic Press New York

[2] Love A E H 1906 *Treatise on the Mathematical Theory of Elasticity* (Cambridge: Cambridge University Press)

[3] Irving J H and Kirkwood J G 1950 *J. Chem. Phys.* **18** 817–29

[4] Hardy R J 1982 *J. Chem. Phys.* **76** 622–8

[5] Murdoch A I 1983 *Q. J. Mechanics Appl. Math.* **36** 163–87

[6] Barenblatt G I 2003 *Scaling* (Cambridge: Cambridge University Press)

[7] Noll W 1955 *Indiana Univ. Math. J. (formerly: J. Ration. Mech. Anal.)* **4** 627–46

[8] Clausius R J E 1870 *Phil. Mag.* **40** 122–7

[9] Maxwell J C 1870 *Trans. R. Soc. Edinburgh* **XXVI** 1–43

[10] Maxwell J C 1874 *Nature* **10** 477–80

[11] Admal N C and Tadmor E B 2010 *J. Elasticity* **100** 63–143

[12] Zimmerman J A, Webb III E B, Hoyt J J, Jones R E, Klein P A and Bammann D J 2004 *Modelling Simulation Mater. Sci. Eng.* **12** S319–32

[13] Goldenfeld N D 1992 *Lectures on Phase Transitions and the Renormalisation Group* (Reading: Perseus Books Publishing, L.L.C.)

[14] Martin J W 1975 *J. Phys. C: Solid State Phys* **8** 2837–57

[15] Evans D J and Holian B L 1985 *J. Chem. Phys.* **83** 4069–74

[16] Reif F 1965 *Fundamentals of Statistical and Thermal Physics* (New York: McGraw-Hill)

[17] LAMMPS (`http://lammps.sandia.gov`)

[18] Daw M S and Baskes M I 1984 *Phys. Rev. B* **29** 6443–53

[19] Zhou X W, Wadley H N G, Johnson R A, Larson D J, Tabat N, Cerezo A, Petford-Long A K, Smith G D W, Clifton P H, Martens R L and Kelly T F 2001 *Acta Mater.* **49** 4005–15

[20] Hoover W G 1985 *Phys. Rev. A* **31** 1695–97

[21] Khinchin A I 1949 *Mathematical Foundations of Statistical Mechanics* (New York: Dover Publications, Inc.)

[22] Hirth J P and Lothe J 1982 *Theory of Dislocations* (New York: John Wiley & Sons Inc) 2 edition

[23] Lazarus D 1949 *Phys. Rev.* **76** 545–53

[24] Gurtin M E 1972 *The Theory of Linear Elasticity (Handbuch der Physik VIa/2)* ed S Flügge (Berlin: Springer)

[25] Webb III E B, Zimmerman J A and Seel S C 2008 *Math. Mech. Solids* **13** 221–66

[26] Eringen A C 1977 *Int. J. Eng. Sci.* **15** 177–83

[27] Lekhnitskii S G 1963 *Theory of Elasticity of an Anisotropic Elastic Body* (San Francisco: Holden-Day, Inc.) originally published as: 1950 *Teoriia Uprugosti Anisotropnovo Tela* (Moscow and Leningrad: Government Publishing House for Technical-Theoretical Works)

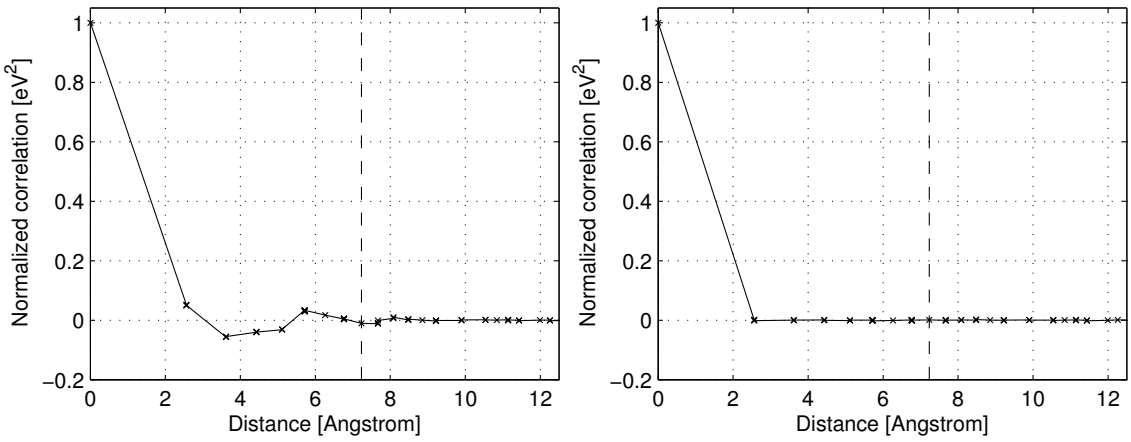

Figure 1. Normalized correlation function of the potential energy (left) and kinetic energy (right) relative to the center atom. The vertical dashed line is at distance $2.00a$ from the center atom.

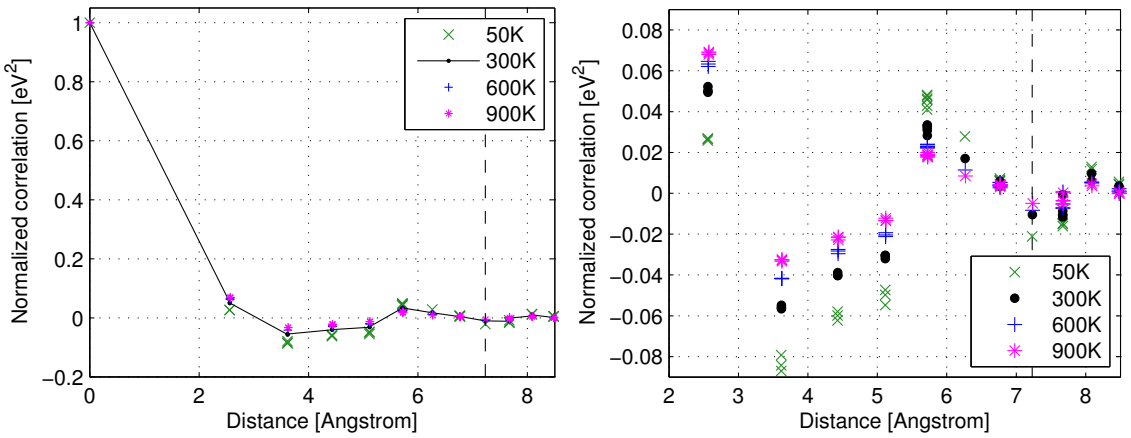

Figure 2. Normalized correlation function of the potential energy at different temperatures relative to the center atom (left) and a magnified plot around the zero-correlation region (right). The vertical dashed line is at distance $2.00a$ from the center atom.

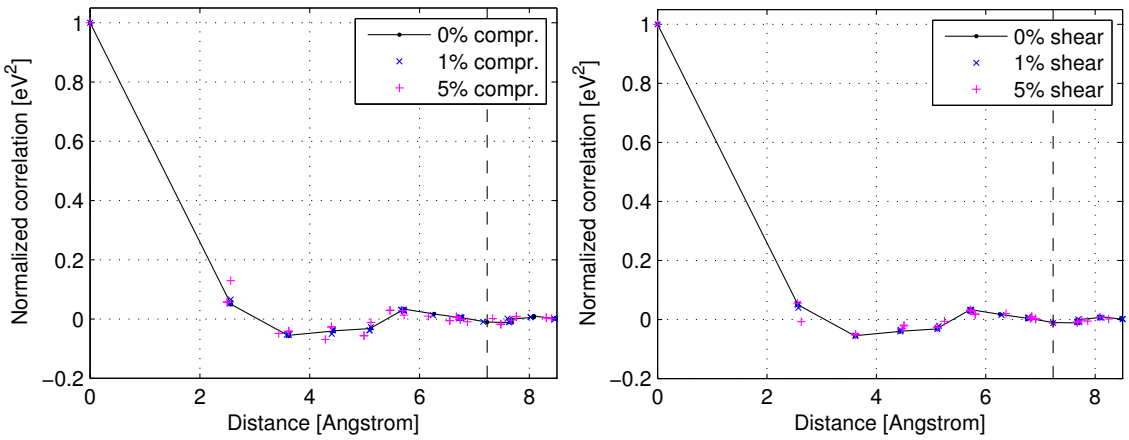

Figure 3. Normalized correlation function of potential energy under compression (left) and shear (right) relative to the center atom. The vertical dashed line is at distance $2.00a$ from the center atom.

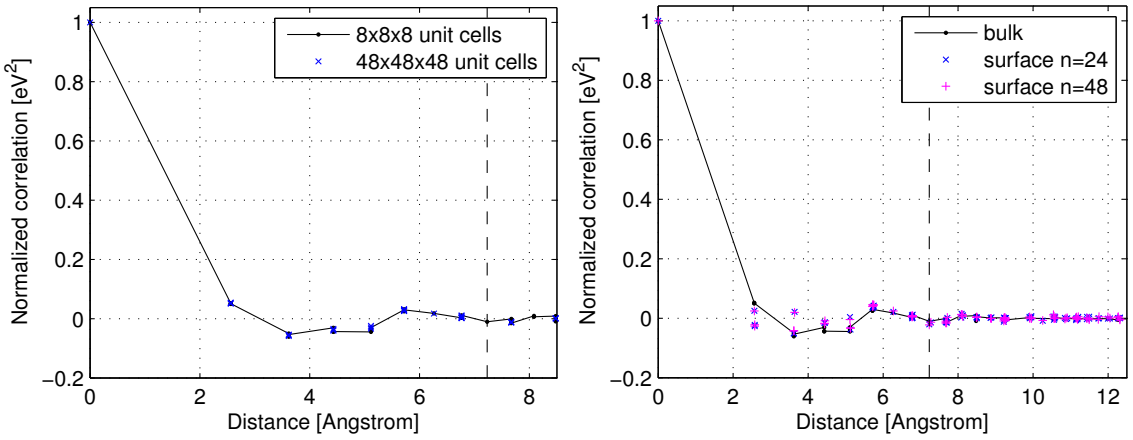

Figure 4. Normalized correlation function of potential energy at no strain. The system size influence on the correlation for the center atom with its neighbors is shown in the left figure, while the surface influence on the correlation for an atom lying on the free surface is shown in the right figure. For the latter, the correlation is considered with the neighbors lying both on the free surface and in the bulk. The vertical dashed line is at distance $2.00a$ from the center atom.

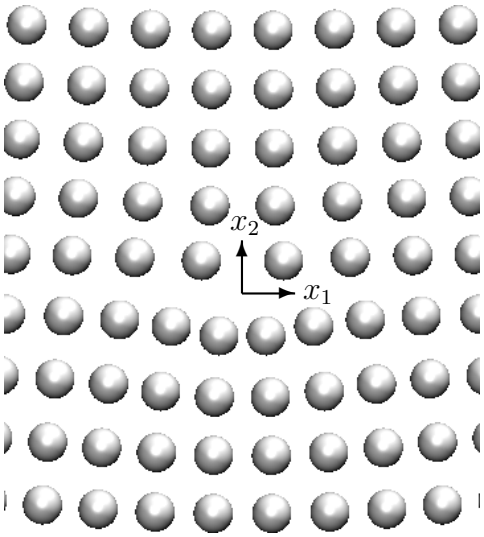

Figure 5. Arrangement of atoms about core of edge dislocation and embedded coordinate system.

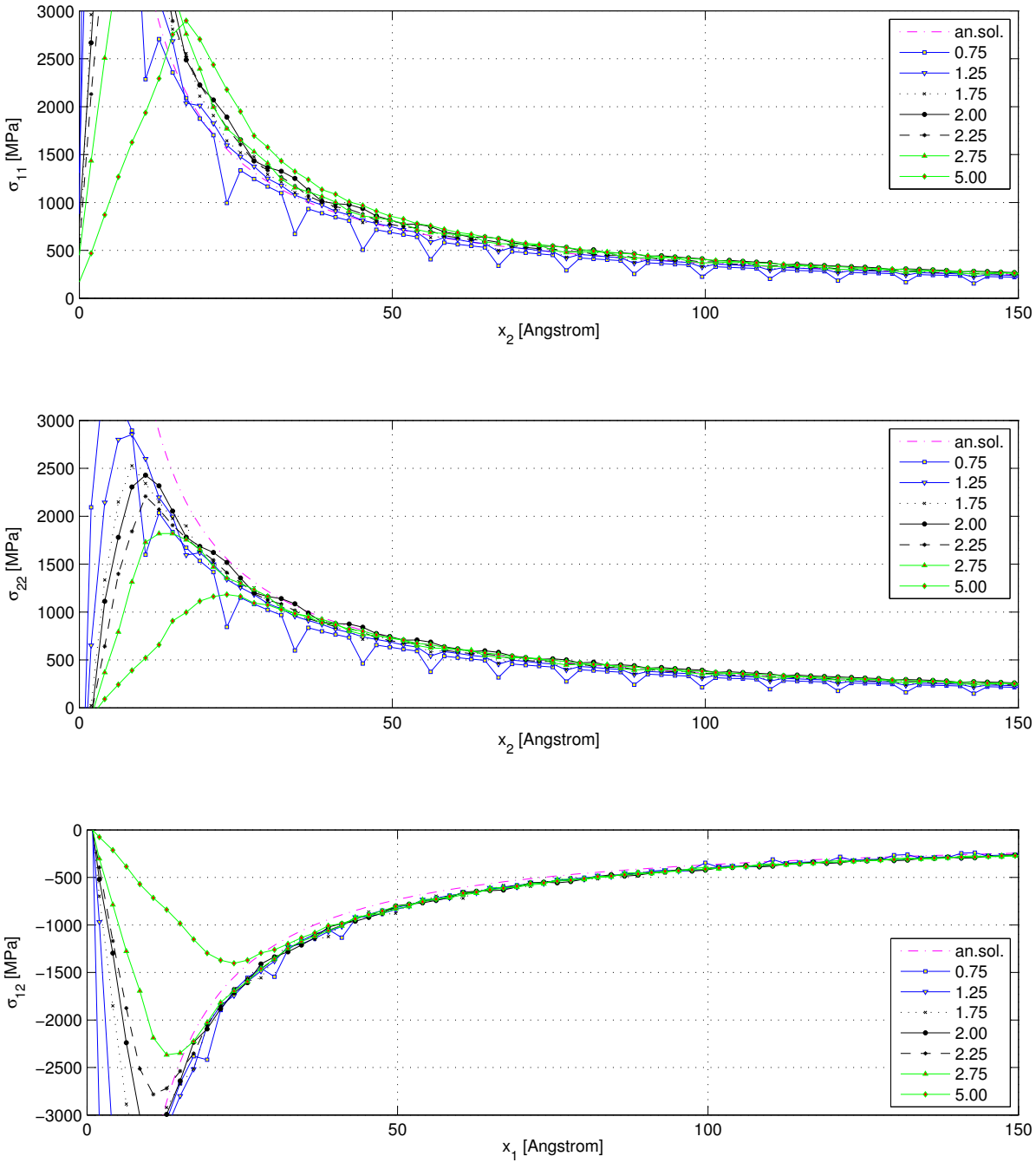

Figure 6. Virial stress distribution about core of edge dislocation. Top: Normal stress σ_{11} in positive x_2-direction at x_1=0; Middle: Normal stress σ_{22} in positive x_2-direction at x_1=0; Bottom: Shear stress σ_{12} in positive x_1-direction at x_2=0. The legends denote radii of cylinders of spatial averaging volume in terms of lattice lengths.

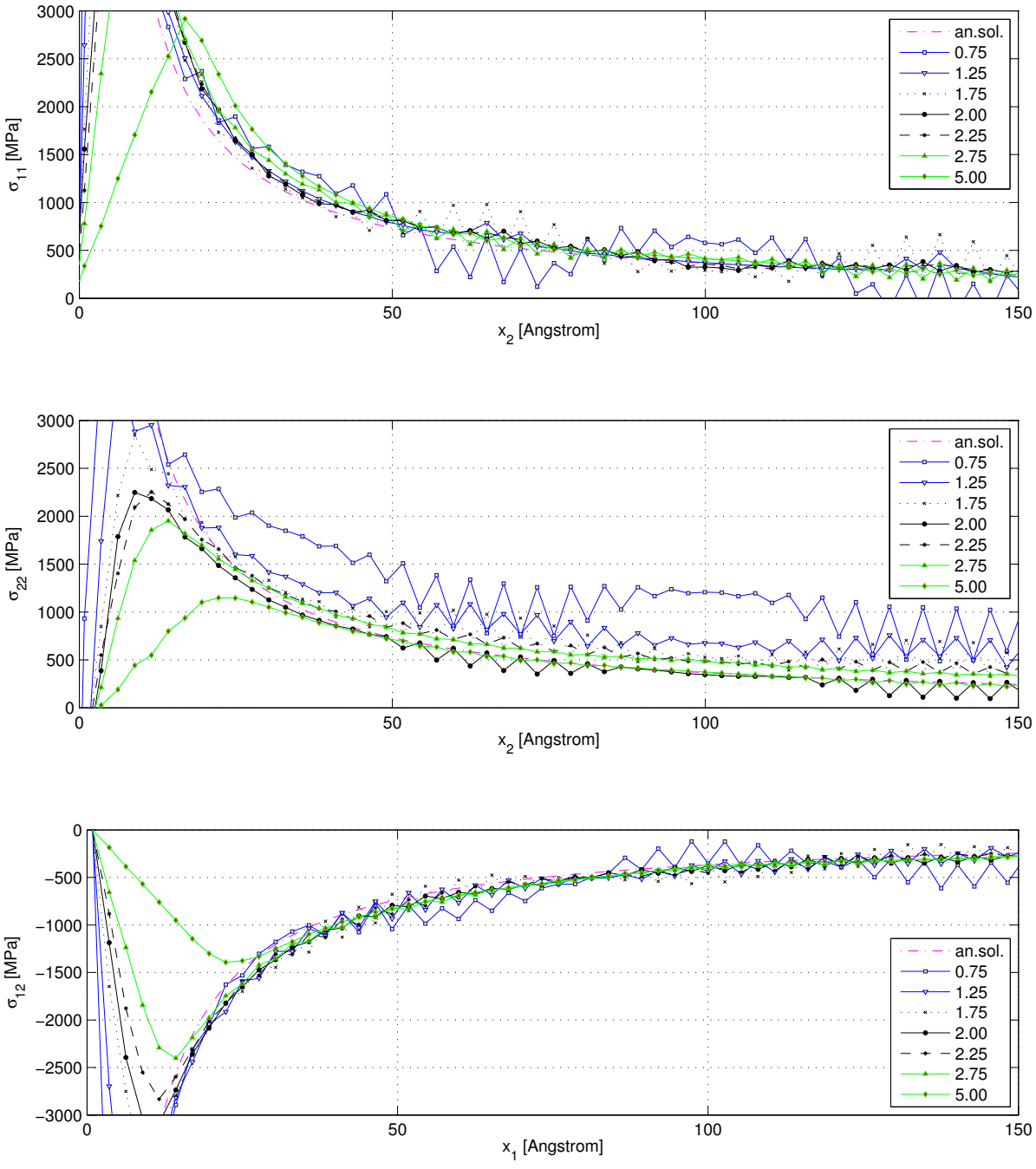

Figure 7. Hardy stress distribution about core of edge dislocation. Top: Normal stress σ_{11} in positive x_2-direction at x_1=0; Middle: normal stress σ_{22} in positive x_2-direction at x_1=0; Bottom: Shear stress σ_{12} in positive x_1-direction at x_2=0. The legends denote radii of cylinders of spatial averaging volume in terms of lattice lengths.

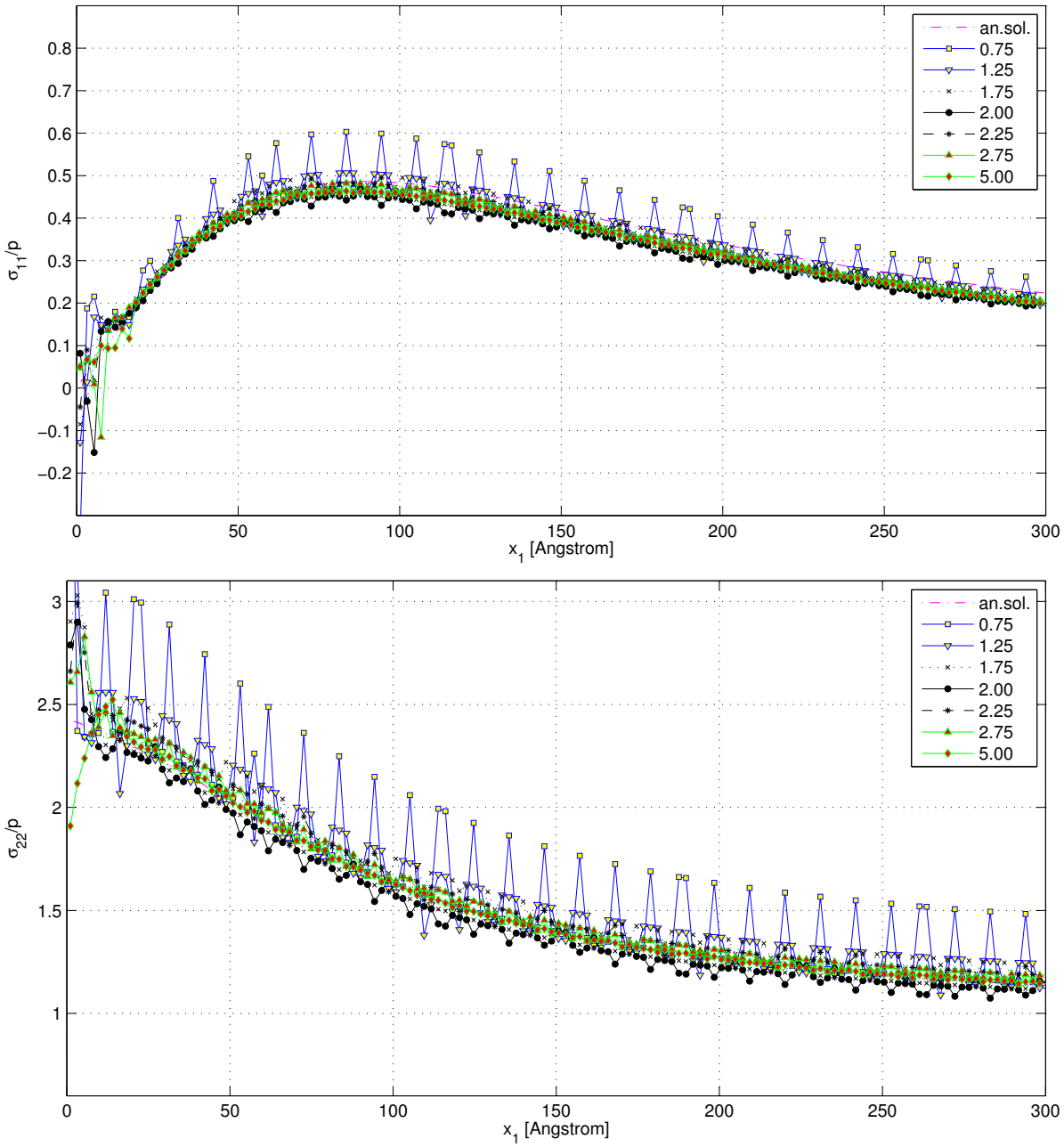

Figure 8. Virial stress distribution for Kirsch problem. Top: Normal stress σ_{11} in positive x_1-direction starting at radius of notch and at x_2=0; Bottom: Normal stress σ_{22} in positive x_1-direction starting at radius of notch and at x_2=0. The legends denote radii of cylinders of spatial averaging volume in terms of lattice lengths.

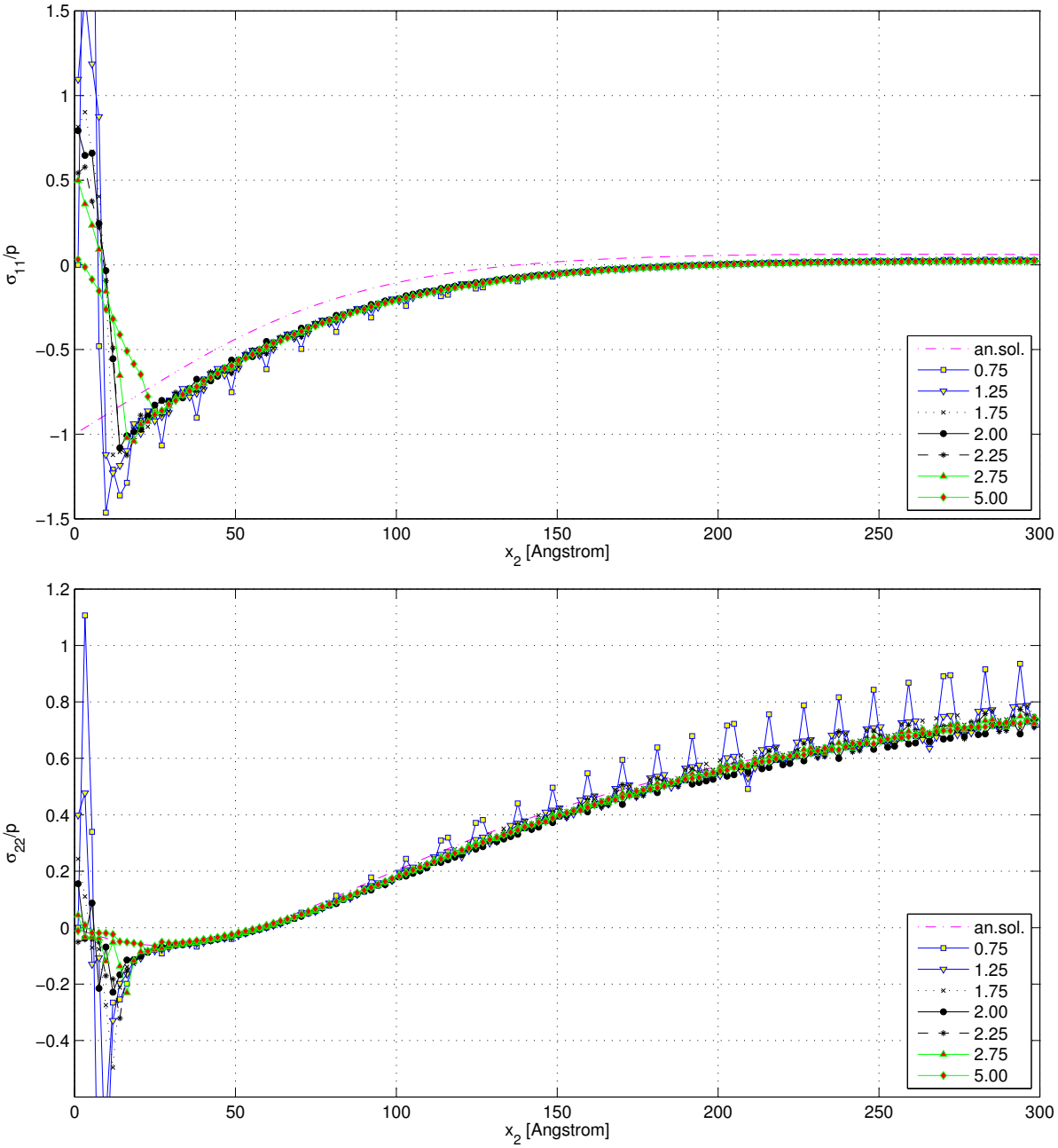

Figure 9. Virial stress distribution for Kirsch problem. Top: Normal stress σ_{11} in positive x_2-direction starting at radius of notch and at x_1=0; Bottom: Normal stress σ_{22} in positive x_2-direction starting at radius of notch and at x_1=0. The legends denote radii of cylinders of spatial averaging volume in terms of lattice lengths.

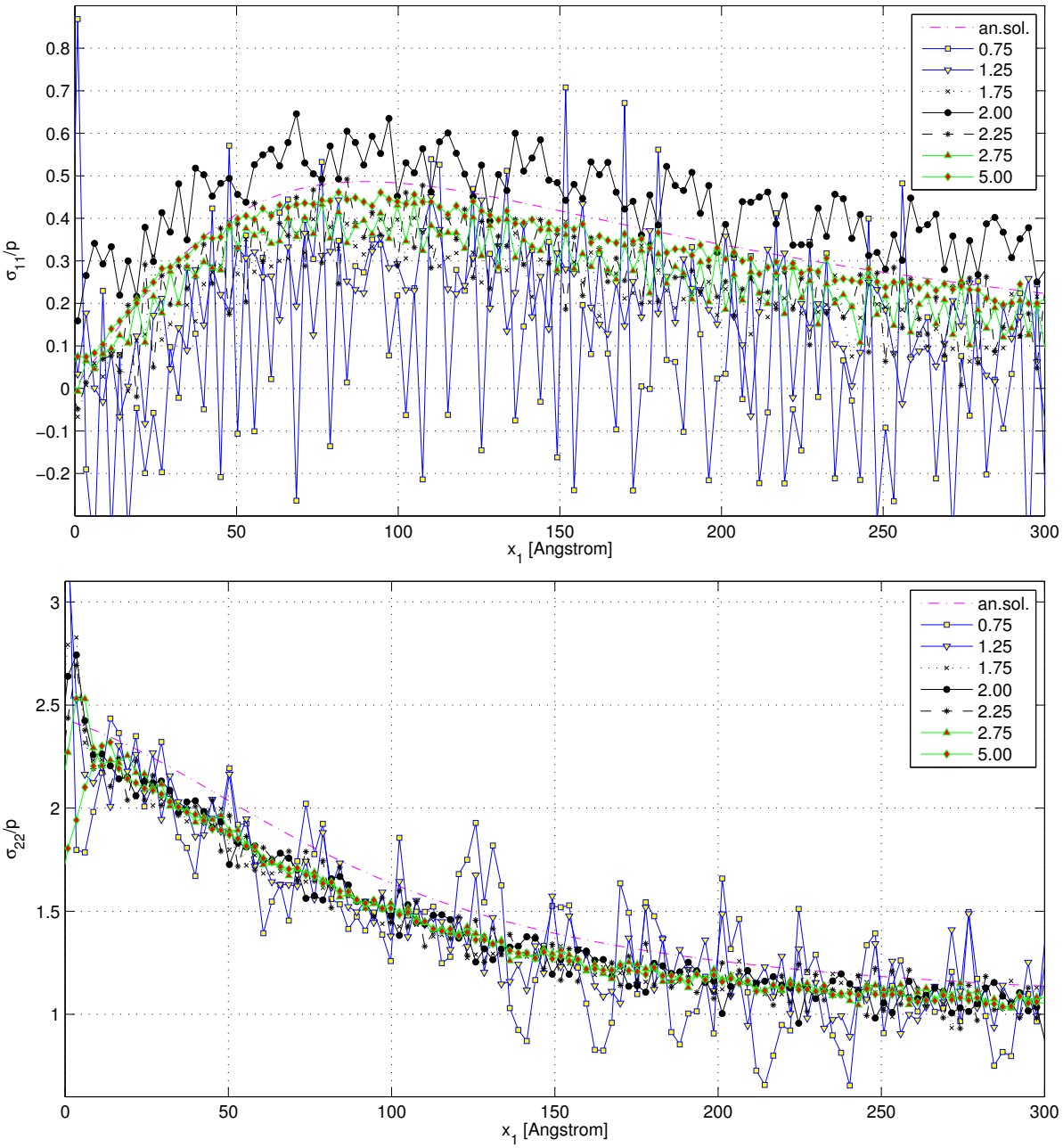

Figure 10. Hardy stress distribution for Kirsch problem. Top: Normal stress σ_{11} in positive x_1-direction starting at radius of notch and at x_2=0; Bottom: Normal stress σ_{22} in positive x_1-direction starting at radius of notch and at x_2=0. The legends denote radii of cylinders of spatial averaging volume in terms of lattice lengths.

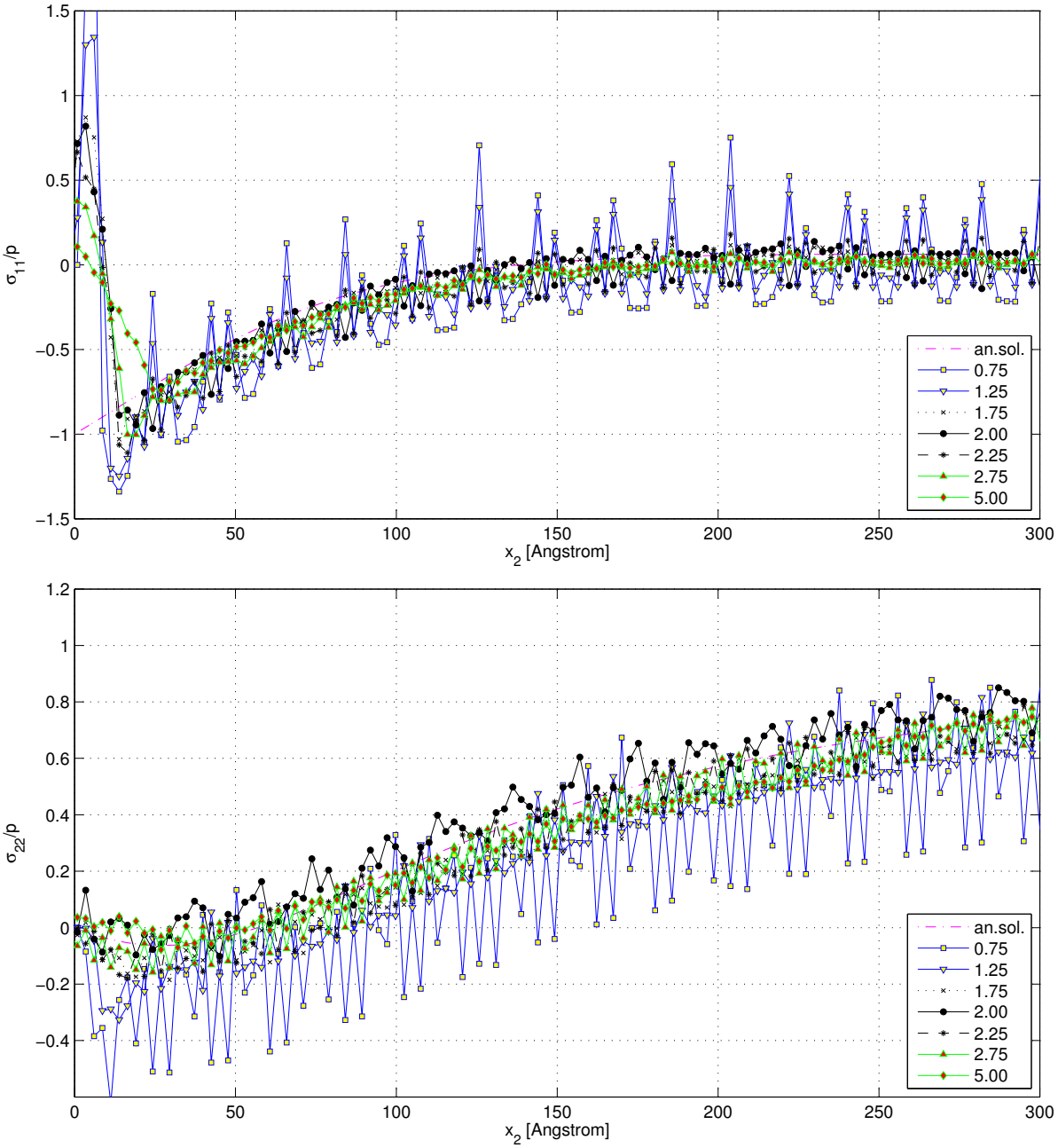

Figure 11. Hardy stress distribution for Kirsch problem. Top: Normal stress σ_{11} in positive x_2-direction starting at radius of notch and at x_1=0. Bottom: Normal stress σ_{22} in positive x_2-direction starting at radius of notch and at x_1=0. The legends denote radii of cylinders of spatial averaging volume in terms of lattice lengths.